Journal of Structural Engineering, ASCE (2017)

Wind-induced vibration mitigation in tall buildings using the tuned mass-damper-inerter (TMDI)

Agathoklis Giaralis[1*], Francesco Petrini[2]

[1] *Department of Civil Engineering, City, University of London, London, UK*

[2] *Department of Structural and Geotechnical Engineering, Sapienza University of Rome, Rome, ITALY*

ABSTRACT

In this paper the classical linear tuned mass-damper (TMD) is coupled with an inerter, a two-terminal device resisting the relative acceleration of its terminals, in various tuned mass-damper-inerter (TMDI) topologies to suppress excessive wind-induced oscillations in tall buildings causing occupants' discomfort. A parametric numerical study is undertaken involving a top-floor-TMD-equipped planar frame capturing accurately the in-plane dynamic behavior of a 74-storey benchmark building exposed to a quasi-stationary spatially-correlated wind-force field accounting for vortex shedding effects in the across-wind direction. It is found that the TMDI reduces the peak top floor acceleration more effectively than the TMD by considering smaller attached mass values, and TMDI topologies in which the inerter spans more stories in linking the attached mass to the host structure. Moreover, the inclusion of the inerter reduces dramatically the TMD stroke while it was verified that the magnitude of the developing inerter forces can be readily accommodated by the host structure. Pertinent illustrative examples are included showcasing that the TMDI meets code-prescribed serviceability design requirements for new tall buildings using significantly smaller attached mass compared to the TMD, and that inerter devices can be used to upgrade the performance of existing TMD-equipped tall buildings without changing the attached mass.

Keywords: *wind-excited tall building, tuned mass damper, inerter, passive vibration control, occupants comfort*

* Corresponding author

INTRODUCTION

Wind-excited slender high-rise buildings with rectangular floor plan are prone to excessive oscillations in the across-wind direction (i.e., within the normal plane to the wind direction) due to vortex shedding effects generated around their edges (Liang et al. 2002). In fact, in many cases, vortex shedding induces higher peak floor accelerations in slender/tall buildings in the across-wind direction than those exhibited in the along-wind direction (Ciampoli and Petrini 2012; Bernardini et al. 2015). In such cases, ensuring that the across-wind floor accelerations remain below a certain threshold associated with users' comfort becomes the critical serviceability design requirement for slender buildings (Kwok et al. 2009).

In this context, over the past three decades, tuned mass-dampers (TMDs) have been widely used in practice, among other devices and configurations for supplemental damping, for vibration mitigation in wind-excited tall buildings to meet occupants' comfort performance criteria prescribed by building codes and guidelines (Kareem et al. 1999; Tse et al 2012). In its simplest form, the linear passive TMD comprises a mass attached towards the top of the building (primary structure), via linear stiffeners, or hangers in case of pendulum-like TMD implementations, and supplemental damping devices (dampers). The effectiveness of the TMD relies on "tuning" its stiffness and damping properties for a given primary structure and attached mass, such that significant kinetic energy is transferred from the vibrating primary structure to the TMD mass and eventually dissipated through the dampers. Focusing on the suppression of lateral wind-induced vibrations in (tall) buildings, the TMD is tuned to the first natural frequency of the primary structure aiming to control the fundamental (translational) lateral mode shape (e.g. Rana and Soong 1998; Li et al. 1999).

It is well-recognized that the vibration suppression capabilities of the TMD depends heavily on its inertial property: the larger the attached TMD mass is, the more effective and robust to uncertainties in the structural properties the TMD becomes (e.g. De Angelis et al. 2012). However, practical structural and architectural constraints apply to the weight and to the volume of the TMD mass that can be accommodated by the primary structure. These constraints are particularly critical for tall buildings for which the attached mass rarely exceeds 0.5% to 1% of the total building mass. In the meantime, in recent years, there is a World-wide trend towards the design and construction of ever-more lighter, slender, and, therefore, more susceptible to wind-induced vibrations tall buildings. This is partly due to the increase cost of land in

congested urban environments and partly due to requirements for more aesthetically pleasing and sustainable structures. Furthermore, the existing TMD-equipped tall buildings risk increase downtime (and consequent financial losses) in the foreseeable future due to an anticipated increase of the frequency of strong wind fronts caused by climate change effects.

To address the above issues and concerns in an innovative manner, this paper explores the potential of incorporating inerter devices to wind-excited TMD-equipped tall buildings in different tuned mass-damper-inerter (TMDI) configurations (topologies) to achieve enhanced vibration suppression in the across-wind direction without increasing the attached TMD mass. Specifically, the considered TMDI topologies, a special case of which was originally introduced in Marian and Giaralis (2013) for seismic protection of multi-storey shear framed structures, benefit from the mass-amplification and from the higher-modes-damping effects of the inerter. The latter is a two-terminal device of negligible mass/weight resisting relative acceleration in analogy to the linear spring and dashpot resisting relative displacement and velocity, respectively (Smith 2002). Marian and Giaralis (2014) showed analytically and numerically that the TMDI can be more effective than the TMD for the same attached mass in reducing the deformation variance of stochastically base-excited linear primary structures due to the contribution of the inerter to the inertial property of the attached mass (mass-amplification effect). Furthermore, Giaralis and Taflanidis (2015) demonstrated that the inclusion of the inerter influences and can potentially suppress higher modes of vibration in linear multi-storey primary structures (higher-modes-damping effect), as opposed to the TMD which can only control a single vibration mode. The latter effect is rather important for wind-induced vibration control in tall buildings since higher vibration modes have a significant contribution to floor acceleration response (i.e., the critical design criterion for tall buildings at the serviceability limit state), as opposed to floor displacements. It is noted in passing that a similar higher-modes-damping effect in linear dynamically excited multi-storey buildings were also reported by Lazar et al. (2014) for the case of the tuned inerter-damper (TID), which is a special case of a TMDI with no attached mass. In fact, this effect was accounted for by Krenk and Høgsberg (2016) to achieve a simplified analytical approach for the optimal TID design targeting a single vibration mode in multi-storey buildings.

Herein, a parametric numerical study is undertaken to assess the effectiveness of different TMDI topologies vis-a-vis the TMD for fixed attached mass in reducing peak top floor displacements and

accelerations in wind-excited tall buildings accounting for vortex shedding effects. To this aim, a 74-storey benchmark building, previously considered in Ciampoli and Petrini (2012) and Spence and Gioffrè (2012), is adopted as a primary structure excited in the across-wind direction by the spatially correlated wind force stochastic model developed by Liang et al. (2002). The structural analysis step is undertaken in the frequency domain and is expedited by modelling the primary structure as a reduced-order lumped-mass linear dynamic system extracted from a detailed finite element (FE). Furthermore, certain practical TMDI design considerations are discussed in view of pertinent numerical results from the parametric study. These include the peak attached mass displacement relative to the peak floor displacement (TMDI stroke), the magnitude of the developing inerter force that needs to be accommodated by the primary structure, and the sizing of the inerter assuming linear device behaviour. A discussion on the latter issue is deemed essential given that: (i) to date, only relatively small-scale inerter devices have been prototyped and tested/characterized (e.g. Papageorgiou and Smith 2005; Wang et al. 2011; Chuan et al. 2012; Swift et al. 2013), or have been made commercially available (Gonzalez-Buelga et al. 2016), tailored for vibration control applications in mechanical/automotive engineering, but not for large-scale civil engineering structures; and (ii) to the authors' best knowledge, this is the first time that inerter devices are considered for wind-induced vibration mitigation in tall buildings. Lastly, the practical advantages and applicability of using inerters to meet code prescribed occupants' comfort serviceability criteria in new and in existing (taken as code-deficient) TMD-equipped tall buildings is numerically illustrated by referring to the adopted benchmark structure.

THE TUNED MASS-DAMPER-INERTER (TMDI) FOR MULTI-STOREY BUILDINGS

Conceptually defined by Smith (2002), the ideal inerter is a linear massless two-terminal mechanical element resisting the relative acceleration at its terminals through the so-called *inertance* coefficient, *b*, measured in mass units. In this regard, the inerter element force *F* shown schematically as a hatched box in the inlet of Fig.1 reads as

$$F = b(\ddot{u}_1 - \ddot{u}_2), \tag{1}$$

where u_1 and u_2 are the axial displacements of the inerter terminals and, hereafter, a dot over a symbol signifies differentiation with respect to time. In view of Eq.(1), the ideal inerter can be interpreted as an inertial weightless element whose gain depends on b and on the relative acceleration observed by its terminals. In fact, in the limiting case of $\ddot{u}_2 = 0$, the inerter behaves as a virtual mass equal to b added to the physical mass of the dynamic degree-of-freedom (DOF) corresponding to the displacement u_1 (Smith 2002). Notably, several different inerter prototypes have been devised and experimentally tested over the past decade achieving inertance values b orders of magnitude larger than the devices' physical mass, while approximating the linear behaviour in Eq.(1) within relatively wide frequency bands of practical interest (e.g. Papageorgiou and Smith 2005; Wang et al. 2011; Li et al. 2012; Swift et al. 2013; Gonzalez-Buelga et al. 2016).

The above considerations led to the TMDI in which an inerter device is used as a mass amplifier contributing additional inertia to the attached mass of the classical TMD without increasing its weight (Marian and Giaralis 2013, 2014). Specifically, consider a planar linear n-storey frame structure modelled as an n-DOF dynamic system with mass m_k (k=1,2,…,n) lumped at the k-th floor as shown in Fig.1. Treating the above system as the primary structure, the TMDI topology introduced by Marian and Giaralis (2013,2014) comprises a mass m_{TMDI} attached to the top floor via a linear spring of stiffness k_{TMDI} and a linear dashpot of damping coefficient c_{TMDI}, and linked to the penultimate floor by an ideal inerter of inertance b. This TMDI topology, shown in Fig.1a, is hereafter termed "-1" as the inerter is linked to one floor below the top floor of the primary structure.

Focusing on wind-excited tall buildings, there is scope in considering alternative TMDI topologies as those in Fig.1(b), "-2", and in Fig.1(c) "-3", in which the inerter spans more than one stories. Such topologies are practically feasible at least for pendulum-like TMDI implementations, which may span more than one storeys by considering sufficiently large slab openings (e.g., Taipei 101 skyscraper). They can potentially achieve more significant engagement of the inerter (i.e., larger inerter forces may develop for the same value of b) as its terminals are less likely to observe in-phase accelerations. Intuitively, this is because the motion of lower floors is less correlated to the motion of the attached mass. Indeed, in a following section (see Fig.2(c) below) it is found that the more floors the inerter spans in a TMDI equipped building,

the more effective the TMDI becomes in suppressing the higher modes of vibration of the primary structure (higher-mode-damping effect).

The mass, **M**, the damping, **C**, and the stiffness, **K**, matrices of a *n*-storey linear frame equipped with a "-p" TMDI topology can be written as

$$\begin{aligned}\mathbf{M} &= \mathbf{M_s^{n+1}} + (m_{TMDI} + b)\mathbf{1_{n+1}}\mathbf{1_{n+1}^T} + b\mathbf{1_{n-p}}\mathbf{1_{n-p}^T} - b\left(\mathbf{1_{n+1}}\mathbf{1_{n-p}^T} + \mathbf{1_{n-p}}\mathbf{1_{n+1}^T}\right)\\ \mathbf{C} &= \mathbf{C_s^{n+1}} + c_{TMDI}\left(\mathbf{1_{n+1}}\mathbf{1_{n+1}^T} + \mathbf{1_n}\mathbf{1_n^T} - \mathbf{1_{n+1}}\mathbf{1_n^T} - \mathbf{1_n}\mathbf{1_{n+1}^T}\right)\\ \mathbf{K} &= \mathbf{K_s^{n+1}} + k_{TMDI}\left(\mathbf{1_{n+1}}\mathbf{1_{n+1}^T} + \mathbf{1_n}\mathbf{1_n^T} - \mathbf{1_{n+1}}\mathbf{1_n^T} - \mathbf{1_n}\mathbf{1_{n+1}^T}\right)\end{aligned}, \quad (2)$$

where n-p is the floor number where the inerter is attached to. In the above expressions, $\mathbf{M_s^{n+1}} \in \mathbb{R}^{(n+1)\times(n+1)}$, $\mathbf{C_s^{n+1}} \in \mathbb{R}^{(n+1)\times(n+1)}$, and $\mathbf{K_s^{n+1}} \in \mathbb{R}^{(n+1)\times(n+1)}$ are the primary structure mass, $\mathbf{M_s} \in \mathbb{R}^{n\times n}$, damping, $\mathbf{C_s} \in \mathbb{R}^{n\times n}$, and stiffness, $\mathbf{K_s} \in \mathbb{R}^{n\times n}$, matrices, respectively, augmented by one last (bottom) row with zero entries and by one last (rightmost) column with zero entries. Further, the vector $\mathbf{1_u} \in \mathbb{R}^{(n+1)\times 1}$ has zero entries except from the u-th entry which is equal to one, and the superscript "*T*" denotes matrix transposition. Note that the inclusion of the inerter device influences only the mass matrix **M** of the controlled structure (i.e., the matrices **C** and **K** are the same for the TMD and for the TMDI). Moreover, note that for *b=0* the mass matrix of a frame building with a TMD attached to the top floor is retrieved (i.e., the TMD is a special case of the TMDI). The latter is the most widely considered TMD topology to control the first (dominant) vibration mode in multi-storey planar frame buildings (Rana and Soong 1998). Furthermore, for $b \neq 0$ the mass matrix **M** in Eq.(2) is not diagonal since the inerter introduces "gyroscopic" inertial cross-terms equal to *-b* that couples the DOF of the attached mass, numbered as *n*+1, with the DOF of the (n-p)-th floor. These cross-terms alter the dynamics of the primary structure such that higher modes of vibration are damped besides the fundamental mode shape. The significance of this higher-mode-damping effect of the TMDI is related to the position of the cross-terms in the matrix **M**: the further away they lie from the main diagonal, the more effective the TMDI becomes in damping the higher modes (see e.g. Fig.2(c)).

As a final remark, the fact that the effective inertia corresponding to the DOF of the attached mass is equal to (m_{TMDI}+*b*) in Eq.(2) (mass amplification effect of the inerter) motivates the definition of the following dimensionless frequency ratio υ_{TMDI} and damping ratio ξ_{TMDI}

$$\upsilon_{TMDI} = \frac{\sqrt{\dfrac{k_{TMDI}}{(m_{TMDI}+b)}}}{\omega_1} \quad , \quad \xi_{TMDI} = \frac{c_{TMDI}}{2\sqrt{(m_{TMDI}+b)k_{TMDI}}}, \tag{3}$$

to characterize the dynamics of the TMDI given an attached mass m_{TDMI} and inertance b. In the last equation ω_1 is the first (fundamental) natural frequency of the primary (uncontrolled) structure.

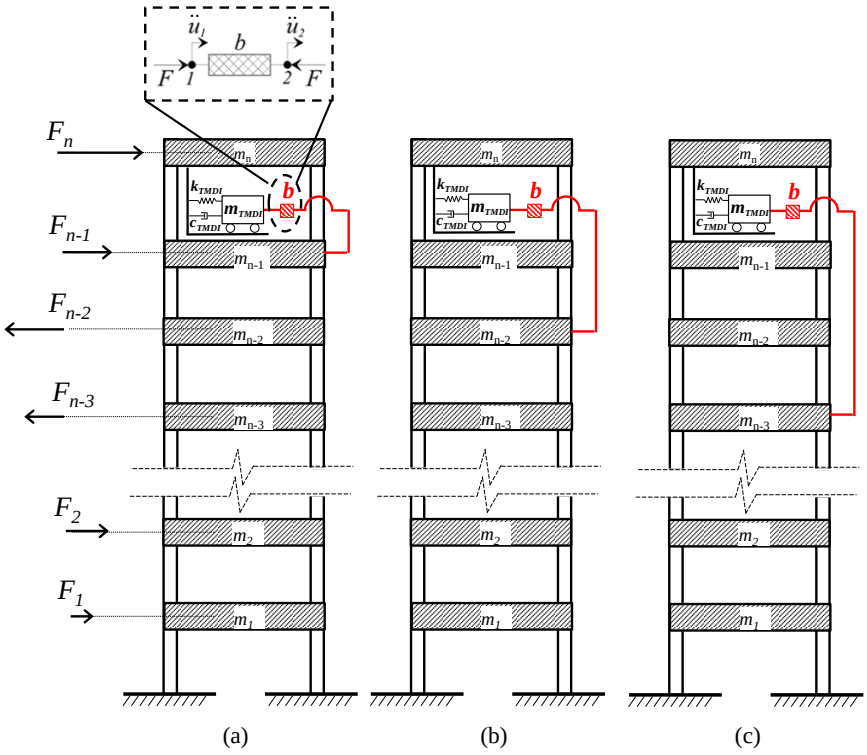

Fig. 1. Lumped-mass linear model of a wind excited n-storey frame building equipped with a tuned mass-damper-inerter (TMDI): (a)"-1" topology; (b)"-2" topology; and (c)"-3" topology.

ADOPTED PRIMARY STRUCTURE AND WIND EXCITATION MODELLING

Benchmark 74-storey building description and detailed FE model

To assess the potential of the TMDI in Fig. 1 for suppressing wind induced oscillations in tall buildings, a high-rise building previously considered for the development of a performance-based wind engineering framework (Spence and Gioffrè 2012; Petrini and Ciampoli 2012) is taken as a benchmark structure. The adopted structure is a 74-storey steel frame building of 305m total height with a 50m-by-50m footprint. Its lateral load resisting system comprises an inner (core) and an outer (perimetric) spatial steel

frames. The two frames are connected by three outriggers located at 100m, 200m, and 300m in elevation. The core frame includes 12 columns, while the perimetric frame has 28 columns. All columns have hollow square sections, with varying outer dimensions and thickness along the building height ranging in between 1.20m to 0.50m, and 0.06m to 0.025m, respectively. Beams are of various standard double-T steel section profiles and all beam-to-column joints are taken as rigid. The outriggers are braces consisted of double-T beams and hollow-square diagonal struts.

A linear FE model of the lateral load resisting structural system of the above benchmark building is shown in Fig.2(a). The model comprises 7592 linear Euler-Bernoulli beam elements with pinned or hinged connections as appropriate. Horizontal perfectly rigid diaphragm constraints are imposed at the height of each floor to account for the effects of the slabs in the model. The mass corresponding to the dead and live loads carried by each slab is uniformly distributed at each floor level. The first three dominantly translational mode shapes along one of the two horizontal principal axes of the (double symmetric in plan) structure are plotted in Fig.2(b). These are obtained from standard linear modal analysis upon constraining all rotational DOFs about the gravitational axis and all translational DOFs along the other horizontal principal axis of the building. The first three natural frequencies of these modes and the corresponding modal participating mass ratios in parentheses are 0.185Hz (0.6233), 0.563Hz (0.1900), and 1.052Hz (0.0745).

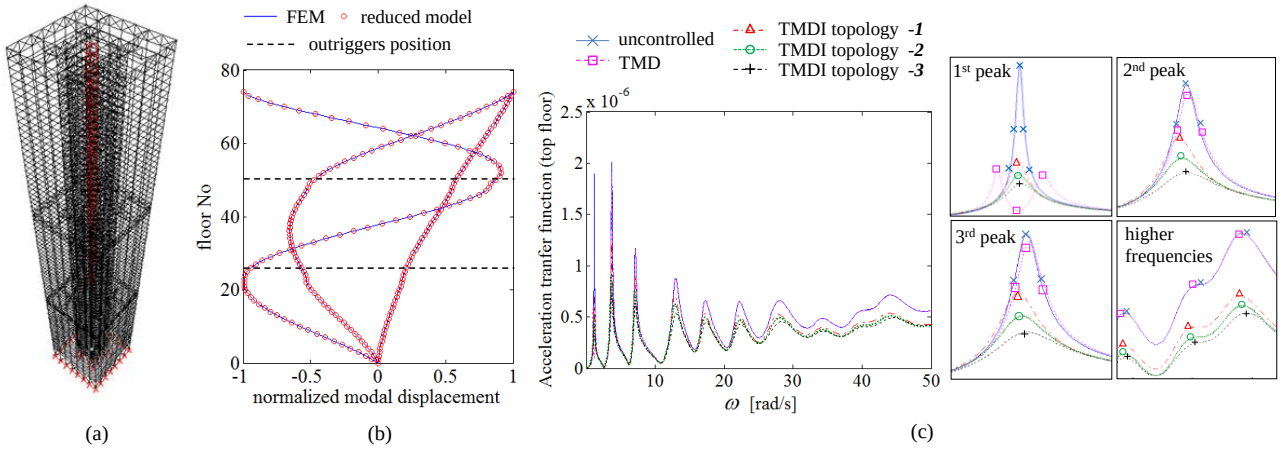

Fig. 2. (a) FE model of the benchmark 74-story building, (b) First three lateral translational mode shapes of the FE model and of the primary structure, (c) Absolute frequency response function of the top floor acceleration of the primary structure, and of four TMD(I)-equipped primary structures.

Primary (uncontrolled) structural system and TMDI-equipped system

A reduced-order dynamic system is next derived from the above discussed FE model which serves as the primary (uncontrolled) structure to expedite the ensuing numerical work (see e.g. Wu et al. 1997). The system has n=74 DOFs and is defined in terms of mass, $\mathbf{M_s} \in \mathbb{R}^{74\times74}$, damping, $\mathbf{C_s} \in \mathbb{R}^{74\times74}$, and stiffness, $\mathbf{K_s} \in \mathbb{R}^{74\times74}$, matrices. The 74 DOFs of the system correspond to the lateral translational DOFs of the FE model in Fig.2(a) along a horizontal (principal) axis of symmetry (see also Yang *et al*. 2004). It is assumed that the building mass is equally distributed along the height of the building and lumped at the center of gravity of the 74 slabs. Under these assumptions, the mass matrix $\mathbf{M_s}$ is diagonal with $M_s(k,k)$=1250ton (k=1,2,…,74) being the mass assigned to each floor. Next, a full stiffness matrix $\mathbf{K_s}$ is obtained such that it satisfies the modal analysis equations

$$\left[\mathbf{K_s} - \omega_{(\mathrm{FE})_j}^2 \mathbf{M_s}\right]\boldsymbol{\varphi}_{(\mathrm{FE})_j} = 0 \quad ; \quad j = 1,2,...,74, \tag{4}$$

where $\boldsymbol{\varphi}_{(\mathrm{FE})_j} \in \mathbb{R}^{74\times1}$ is the j-th translational mode shape along a principal building axis discretized at the slab heights and $\omega_{(\mathrm{FE})j}$ is the corresponding natural frequency obtained from modal analysis applied to the detailed FE model discussed in the previous section. The thus derived $\mathbf{K_s}$ and $\mathbf{M_s}$ matrices capture well the first 74 lateral translational mode shapes and natural frequencies along a principal building axis as obtained by the FE model in Fig.2(a). For illustration, the first three normalized mode shapes obtained from the FE model, $\boldsymbol{\varphi}_{(\mathrm{FE})j}$ (j=1,2,…,6) and from the reduced 74-DOF dynamical system $\boldsymbol{\varphi}_j$ (j=1,2,…,6) are superposed in Fig.2(b) shown to match very well. Lastly, a full damping matrix is obtained by the expression (Chopra 2000)

$$\mathbf{C_s} = \left(\boldsymbol{\Phi}^T\right)^{-1} \mathbf{C}_{\mathrm{mod}} \left(\boldsymbol{\Phi}\right)^{-1}, \tag{5}$$

where $\boldsymbol{\Phi} \in \mathbb{R}^{74\times74}$ is the modal matrix collecting all the 74 $\boldsymbol{\varphi}_j$ mode shapes of the 74-DOF dynamical system and the superscript "-1" denotes matrix inversion. In the last equation, $\mathbf{C_{mod}} \in \mathbb{R}^{74\times74}$ is a diagonal matrix collecting the modal damping coefficients in its main diagonal as in

$$\mathbf{C_{mod}}[j,j] = 2\omega_j\xi_j\left(\boldsymbol{\varphi}_j{}^T \mathbf{M_s} \boldsymbol{\varphi}_j\right) \quad ; \quad j = 1,2,...,74. \tag{6}$$

In the above equation, ω_j is the j-th natural frequency of the considered 74-DOF dynamical system, and ξ_j is the j-th modal damping ratio of the system, taken equal to: ξ_j=2%, for j= 1,2,3; ξ_j= 4% for j= 4,5,6; ξ_j= 6% for j= 7,8,9,10; ξ_j=9% for j= 11,12,…,20; ξ_j=12% for j= 21,22,…,40; ξ_j=15% for j=41,42,…,60; and ξ_j=18% for j=61,62,…,74. These damping ratio values follow closely pertinent field-recorded data for tall steel framed buildings reported in the literature for the frequency range of 0-7Hz (Satake et al. 2004; Spence and Kareem 2014). For natural frequencies above this range, increasing damping ratios with natural frequency are assumed converging asymptotically to an arbitrarily taken 18% damping ratio. The assumed increase of damping with frequency trend accounts for the anticipated greater participation of non-structural components to the inherent damping of the structure for oscillations dominated by the higher vibration modes (see e.g., Spence and Kareem 2014 and references therein).

Note that the choice to consider such a large number of translational horizontal DOFs equally spaced along the height of the building model was made to capture accurately the influence of the stiff outriggers to the local dynamics of the structure (see Fig.2b), and to facilitate a fine spatial discretization of the wind loading. Moreover, this choice enables the incorporation of a TMDI with any "-p" topology to the primary structure as suggested by Eq.(2), since the translational DOFs corresponding to all the upper building floors are maintained (see also Fig.1). In particular, the four inerter contributing terms for a given TMDI topology can be readily added to the augmented $\mathbf{M}_{\mathbf{s}}^{75} \in \mathbb{R}^{75\times75}$ mass matrix in Eq.(2) to form $\mathbf{M} \in \mathbb{R}^{75\times75}$ mass matrices for the TMDI-equipped adopted benchmark structure along one principal direction. In this fashion, the fact that, to the best of the authors' knowledge, no FE software package currently exist with explicit inerter modelling capabilities is by-passed. Furthemore, a frequency domain approach, as detailed in the following section, can be adopted to determine peak structural response quantities to wind excitation in a computationally efficient manner using the **M**, **C**, and **K** matrices in Eq.(2) to represent the TMDI-equipped primary structures. This structural analysis step can be readily implemented in any high-level computer language, such as MATLAB®, to account for the contribution of all the higher modes to the (peak) structural response. The latter consideration is important for the purposes of this work as the TMDI topology influences significantly all higher modes of the primary system. This issue is illustrated in Fig.2(c) for the case of three TMDIs with the same properties but with the different topologies shown in Fig.1. This aspect

constitutes yet another reason for choosing to consider a primary structural system with 74 DOFs corresponding to all 74 floor translational DOFs of the adopted benchmark building.

Wind excitation model and frequency domain analysis for the TMDI-equipped system

The wind action is considered only in the across-wind direction along a principal horizontal axis of the adopted benchmark building as this is the critical direction to check for the occupants' comfort criterion for this particular structure (Ciampoli and Petrini 2012). The wind force components F_k (k=1,2,…,74) acting at the slab heights of the primary structure as pictorially shown in Fig.1 are modelled as a zero-mean Gaussian ergodic spatially correlated random field represented in the frequency domain by a $\mathbf{S}_{\mathbf{FF}}^{\mathbf{74}}(\omega) \in \mathbb{R}^{74\times 74}$ power spectral density (PSD) matrix. Among other models proposed in the literature (e.g. Simiu and Scanlan 1978, Kareem 1982, Vickery and Basu 1983), the stochastic wind field model of Liang et al. (2002) is herein adopted to define the across wind force PSD matrix $\mathbf{S}_{\mathbf{FF}}^{\mathbf{74}}$. The considered model relies on experimental wind tunnel data pertaining to scaled prototypes of rectangular high-rise buildings of various side ratios in plan-view. It accounts for wind turbulence and vortex shedding effects as well as spatial correlation. The considered benchmark building has a square floor plan and, therefore, the 1:1 side ratio case is taken in evaluating the elements of the $\mathbf{S}_{\mathbf{FF}}^{\mathbf{74}}$ matrix using the formulae reported in Liang et al. (2002). For illustration, across-wind force PSD functions evaluated at the height of three different floors are plotted in Fig. 3 for top floor mean wind velocity V_{ref}= 35m/s.

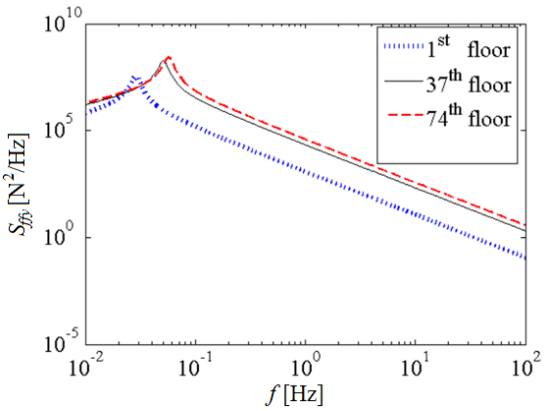

Fig. 3. Considered across-wind force spectra at three different floor heights.

The response displacement and acceleration PSD matrices of the TMDI-equipped primary structure defined by the **M**,**C**, and **K** matrices in Eq.(2) due to the $\mathbf{S}_{\mathbf{FF}}^{\mathbf{74}}$ matrix are obtained using the frequency domain input-output relationships of random vibrations (e.g. Soong and Grigoriu 1993)

$$\mathbf{S}_{\mathbf{xx}}(\omega)=\mathbf{B}(\omega)^{*}\,\mathbf{S}_{\mathbf{FF}}(\omega)\mathbf{B}(\omega) \quad \text{and} \quad \mathbf{S}_{\ddot{\mathbf{x}}\ddot{\mathbf{x}}}(\omega)=\omega^{4}\mathbf{S}_{\mathbf{xx}}(\omega), \tag{7}$$

respectively. In Eq. (7), $\mathbf{S}_{\mathbf{FF}}$ is the PSD wind force matrix $\mathbf{S}_{\mathbf{FF}}^{\mathbf{74}}$ augmented by a zero row and a zero column corresponding to the DOF of the TMDI which is not subjected to any wind load (internally housed). Further, the "*" superscript denotes complex matrix conjugation, and the transfer matrix **B** is given as

$$\mathbf{B}(\omega)=\left[\mathbf{K}-\omega^{2}\mathbf{M}+i\omega\mathbf{C}\right]^{-1}, \tag{8}$$

where, $i=\sqrt{-1}$. Next, the response displacement and acceleration variances of the *k*-th floor for the TMDI-equipped primary structure are obtained as

$$\sigma_{x_k}^{2}=\int_{0}^{\omega_{\max}} S_{x_k x_k}(\omega)\,d\omega \quad \text{and} \quad \sigma_{\ddot{x}_k}^{2}=\int_{0}^{\omega_{\max}} S_{\ddot{x}_k \ddot{x}_k}(\omega)\,d\omega, \tag{9}$$

respectively. That is, by integrating the response auto-spectra populating the main diagonal elements of the response PSDs in Eq. (7) on the frequency axis up to a maximum (cut-off) frequency ω_{max} above which the energy of the underlying processes is negligible. Furthermore, the variance of the relative acceleration response between two different floors (or DOFs) *k* and *q*, $\ddot{x}_k-\ddot{x}_q$, is obtained by (e.g., Soong and Grigoriu 1993)

$$\sigma_{\ddot{x}_{kq}}^{2}=\sigma_{\ddot{x}_k}^{2}+\sigma_{\ddot{x}_q}^{2}-2\int_{0}^{\omega_{\max}} S_{\ddot{x}_k \ddot{x}_q}(\omega)\,d\omega, \tag{10}$$

where the integrand is the acceleration response cross-spectrum corresponding to the *k* and *q* DOFs. Finally, peak *k*-th floor displacements and accelerations and peak relative acceleration between *k* and *q* floors, are estimated by the expressions

$$\max\{x_k\}=g\sqrt{\sigma_{x_k}^{2}}, \quad \max\{\ddot{x}_k\}=g\sqrt{\sigma_{\ddot{x}_k}^{2}}, \quad \text{and} \quad \max\{\ddot{x}_{kq}\}=g\sqrt{\sigma_{\ddot{x}_{kq}}^{2}}, \tag{11}$$

respectively. In the above expressions, g is the peak factor estimated by the widely used empirical formula due to Davenport (1964)

$$g = \sqrt{2ln\left(\eta T_{wind}\right)} + \frac{0.577}{\sqrt{2ln\left(\eta T_{wind}\right)}}, \tag{12}$$

where $\eta=2\pi/\omega$ is the effective structural response frequency in Hz (e.g., can be taken equal to the fundamental natural frequency of the primary structure), and T_{wind} is an assumed time duration of exposure to the wind action during which the peak response quantities in Eq.(11) are evaluated. The latter consideration implies that the underlying stochastic input/output processes are quasi-stationary (i.e., stationary/ergodic time-limited processes). In the following sections, the peak response quantities in Eq.(11) are used to assess the effectiveness of the TMDI to suppress wind induced vibrations in tall buildings.

ASSESSMENT OF TMDI VIBRATION SUPPRESSION CAPABILITIES VIS-À-VIS THE TMD

In this section, a parametric investigation is undertaken to quantify the effectiveness of different TMDI topologies to mitigate vibrations in the across-wind direction of tall buildings accounting for vortex shedding effects. To this aim, the previously discussed 74-DOF structural system is taken as a paradigm of a primary structure exposed to wind loading modelled by the adopted $\mathbf{S}_{\mathbf{FF}}^{\mathbf{74}}$ PSD matrix for top floor mean wind velocity V_{ref}= 35m/s (Fig.3). In evaluating the peak factor, g, in Eq.(12), a one hour of wind exposure, T_{wind} = 3600s, is assumed, for which g= 3.76 taking the characteristic frequency η equal to the fundamental natural frequency of the primary (uncontrolled) structure.

The response factors (RFs) for the peak top floor displacement and acceleration of the primary structure for the three different TMDI topologies of Fig.1 are plotted in Fig. 4 as functions of the inertance ratio $\beta=b/M$ and for seven different attached mass ratio values $\mu= m_{TMDI}/M$, where M is the total mass of the primary structure. These RFs are obtained by normalizing the peak response quantities in Eq. (11) by the corresponding values of the uncontrolled structure, while the inertance ratio is let to vary in the range of 0% to 100% of the primary structure mass, with the special case of β=0 being the TMD. The values of the TMDI frequency and damping ratios in Eq.(3) have been determined by the expressions

$$\upsilon_{TMDI} = \frac{\sqrt{1+0.5(\beta+\mu)}}{1+\beta+\mu} \quad \text{and} \quad \xi_{TMDI} = \sqrt{\frac{(\beta+\mu)\left[1+0.75(\beta+\mu)\right]}{4(1+\beta+\mu)\left[1+0.5(\beta+\mu)\right]}}, \tag{13}$$

respectively. The above formulae yield optimal tuning parameters for the classical TMD with attached mass $\mu+\beta$ minimizing the displacement response variance of white noise force-excited undamped single DOF primary structures (Wartburton 1982). In this regard, the expressions in Eq.(13) do not achieve, by any means, optimum TMDI designs for the herein adopted primary structure against any particular optimization criterion. Still, they do yield reasonable values for the stiffness and the damping properties of the TMDI, accounting for the mass amplification effect of the inerter, which suffice to draw valid and useful comparisons of the effectiveness of different TMDI topologies vis-à-vis the TMD (β=0) case.

From the first row of plots in Fig. 4, it is seen that the inclusion of the inerter is beneficial in terms of reducing the peak top floor displacement compared to the TMD, only for relatively small attached mass values. In fact, in the case of the "-1" TMDI topology and for $\mu \geq 0.5\%$, the classical TMD outperforms the TMDI for the whole range of β values considered. However, the TMDI efficiency in peak top floor displacement reduction increases appreciably as TMDI topologies in which the inerter spans more and more storeys are considered. For such topologies, the inclusion of a relatively small value of inertance renders the TMDI significantly more efficient than the TMD. For example, by adding an inerter of β=10% in the "-3" topology to a TMD with μ=0.1% achieves a further 8.75% reduction to the peak top floor displacement of the uncontrolled structure. Nevertheless, the rate of RF decrease tends to saturate for increased inertance values. These trends are in alignment with results reported in the literature for the case of earthquake excited low-rise building structures (Marian and Giaralis 2013, 2014).

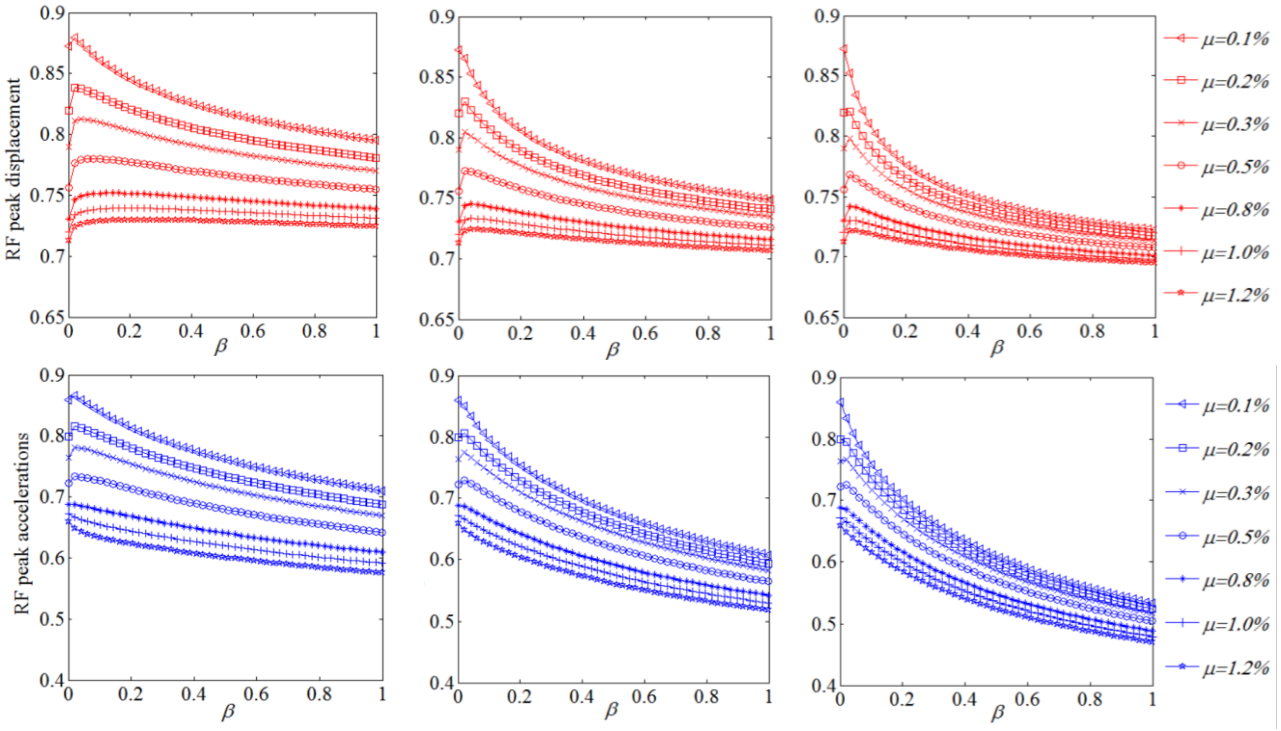

Fig. 4. Peak top floor displacement (upper panels) and acceleration (bottom panels) of TMDI equipped primary structure for different inertance ratio, β, and attached mass ratio, μ, values normalised by the corresponding peak values of the uncontrolled structure for TMDI topologies (a)"-1", (b)"-2", and (c)"-3".

Turning the attention to the lower row of plots in Fig. 4, it is seen that the TMDI does considerably better from the classical TMD in mitigating the peak top floor accelerations which is the critical serviceability design performance parameter for wind-excited tall building. Specifically, for all the values of the attached mass considered, improved peak top floor acceleration reduction is achieved with higher inertance values. For larger attached masses, the improvement to the acceleration RFs is monotonic, but tends to saturate faster and is less significant compared to smaller attached mass. Lastly, significantly smaller RFs are achieved for TMDI topologies with inerters attached to lower floors.

The fact that the herein considered non-optimal TMDIs are better suited to suppress floor accelerations rather than floor displacements, compared to the TMD, is readily attributed to the higher-mode-damping effect of the TMDI. Indeed, the TMDI suppresses not only the portion of the structural vibration response corresponding to the fundamental mode shape, as the TMD strictly does, but all higher modes as well, which contribute significantly more to response acceleration than to response displacement. For illustration, Fig.2(c) plots the absolute frequency response functions (FRFs) of the top floor acceleration

(i.e., the $B(74,74)$ element in Eq. (8) multiplied by ω^2) of primary structures equipped with TMDIs of the same properties but different topologies and a same-attached-mass TMD-equipped primary structure. The corresponding FRF of the uncontrolled structure is superposed: it coincides with the FRF of the TMD-equipped structure for frequencies higher than the fundamental natural frequency of the primary structure, but not with the FRFs of the TMDI-equipped structures whose ordinates lie appreciably lower across all frequencies. Importantly, the lower the p floor the inerter is attached to, the more significant damping the TMDI achieves to all primary structure modes.

Overall, the herein reported numerical data suggests that the incorporation of the inerter to the TMD is rather beneficial in reducing floor accelerations and that the smaller the attached mass is the more significant this reduction becomes. The first observation paves the way for considering inerters to *retrofit/upgrade* the performance of existing TMD-equipped tall buildings. The second observation facilitates the design of new tall buildings achieving the same level of structural performance with significantly reduced attached mass. Both these points are numerically illustrated in a subsequent section, but first, in the following section, certain important practical aspects on the TMDI design and implementation are discussed.

SOME PRACTICAL DESIGN CONSIDERATIONS FOR TMDI-EQUIPPED TALL BUILDINGS

Having established the potential benefits of coupling TMDs with inerters to control wind-induced vibrations in tall buildings, it is herein deemed important to discuss certain practical design considerations for TMDI-equipped tall buildings related to the attached mass relative displacement (TMDI stroke), the inerter force, and the required size and weight of ideal inerter device realizations for the application at hand. To study the effect of the inerter to the attached mass displacement, the first row of panels in Fig. 5 plot the peak attached mass displacement relative to the peak top floor displacement for the same cases of TMDI-equipped primary structure considered in Fig.4 normalized by the peak attached mass displacement of the TMD (β=0 case). Evidently, the inclusion of the inerter device reduces dramatically the TMDI stroke (note the logarithmic scale of the y-axis in the considered plots), though the reduction rate reduces as the inertance value increases for the same attached mass. Further, the TMDI topology does affect the amplitude of the stroke (but not the trends for increasing inertance): the more stories the inerter spans the higher the peak stroke is for the same TMDI properties. In every case, the inclusion of the inerter is quite beneficial in

reducing the peak attached mass relative displacement and this reduction is greater for smaller attached masses. This is a significant advantage of the TMDI over the TMD as it relaxes the stroke requirements for the damper, as well as the required clearance between the attached mass and the primary structure to avoid pounding, which are often become critical in TMD design (see e.g. Wang et al. 2009).

Based on force equilibrium considerations, the above discussed stroke reduction is readily attributed to the inerter force in Eq. (1) applied to the attached mass. In this respect, it is important to gauge the peak value of this force as it needs to be locally accommodated by the primary structure at the p floor. To this end, in the lower row of panels in Fig. 5 the peak inerter force is plotted as a function of the inertance ratio for fixed attached mass ratios. It is seen that the inerter force increases rapidly with the inertance up to a critical inertance ratio value ranging between 15% to 25% depending primarily on the attached mass and less on the TMDI topology. Above this critical value, the inerter force increases further, but at a significantly lower rate for TMDI topologies with p>1 and for relatively large attached mass values, while for the "-1" topology it decreases with the inertance for all the attached mass values considered. In all cases, for a given inertance, the peak inerter force reduces significantly for reduced attached mass (e.g., it is about 30kN for μ=0.1%), while even in the worst case scenario of the "-1" topology with μ=1.2% it attains a maximum value of about 100kN. In this respect, no special provisions (or excessive cost for that matter) for the inerter-to-the-primary-structure local connection is required beyond those considered in accommodating the commonly observed forces developed in energy dissipation devices used for the seismic protection of steel framed buildings (Karavasilis et al. 2011). Moreover, this connection can be made sufficiently stiff such that negligible compliance is observed for the anticipated inerter force F in Eq.(1). This consideration can be further facilitated by using more than one inerter devices in parallel such the total force demand F is split into several inerter devices, each one transferring a significantly smaller than F force to the connection with the primary structure.

A further practical concern to be addressed in discussing the feasibility of the TMDI for wind-induced vibration control in tall buildings relates to the required inerter size and specifications. To this end, note that the only commercially available inerter device is tailored for vehicle suspension systems control and, therefore, is rather compact weighting about 2kg and achieving an inertance of about 75kg as reported in Gonzalez-Buelga et al. (2016). Nevertheless, also note that with few exceptions (Swift et al. 2013), the

typical inerter prototypes discussed in the literature employ either mechanical arrangements (e.g. rack-and-pinion or ball-screw mechanisms) (Papageorgiou and Smith 2005; Li et al. 2012) or hydraulics-based principles (Wang et al. 2011) to transform the translational kinetic energy into rotational kinetic energy stored in a "flywheel": a lightweight fast-spinning disk. Importantly, the value of the inertance *b* is primarily dependent on the flywheel rotational inertia and allowed tangential velocity, rather than on its mass. The fact that the angular velocity of the flywheel can be arbitrarily regulated through, for example, mechanical gearing (e.g. Smith 2002), renders the inertance be practically independent from the device physical mass. For illustration, Table 1 collects numerical data pertaining to the preliminary sizing of the flywheel, taken as a solid steel disk, in the inerter devices involved in three particular TMDIs examined in Fig.4. Specifically, an energy approach is used assuming no losses and linear device behaviour in which it is sought to determine the required flywheel radius given a pre-specified flywheel thickness and flywheel tangential velocity. The input energy to be accommodated (stored) by the flywheel is computed as the product of the peak inerter force in Fig.4 times the peak relative displacement at the inerter terminals, which yields a conservative value as these two quantities do not peak simultaneously. A flywheel thickness of 0.02m is assumed in all cases, while the peak tangential velocity is purposely fixed to a low value of 50m/s; i.e. an order of magnitude lower than the maximum value that a steel disk can attain without developing excessive stresses leading to high-cycle or even low-cycle fatigue failure (Pullen and Dhand 2014). Therefore, the herein sized flywheels have a large safety margin and may well accommodate more severe wind velocity fields than the one adopted in the previous section corresponding to V_{ref}=35 m/s. It is seen that in all cases considered the required flywheels weight less than 6kg and have a diameter of less than 22cm. Such flywheels can be readily manufactured and be safely encased and housed in a tall building. Similar conclusions hold for the gearing system that could be used to drive such a flywheel as the input power (product of inerter peak force times peak relative inerter terminals' velocity) is much lower than the power accommodated by gearing mechanisms in typical wind turbines used for renewable energy production. However, note that, besides gearing, other mechanisms are utilized to drive a flywheel in current inerter devices (e.g. Wang et al. 2011), while there exist inerter realizations which do not rely on a flywheel (Swift et al. 2013; Gonzalez-Buelga et al. 2015), and might be better amenable to scaling-up. In this regard, it is emphasized that the flywheels reported in Table 1, assumed to be driven by a gearbox, should not be interpreted as a recommended solution

for an actual large-scale inerter device, but rather as a demonstration that inerter devices required in TMDIs to control wind-induced oscillations in tall buildings are physically realizable.

As a final remark, it is noted that throughout this work ideal linear inerter behaviour is assumed. Nevertheless, deviations from the ideal linear inerter behavior have been experimentally observed during testing of various small-scale prototypes (Papageorgiou and Smith 2005; Li et al. 2012; Swift et al. 2013) and of the commercially available inerter (Gonzalez-Buelga et al. 2016). These deviations are attributed to several different factors associated with the underlying technology used in the inerter implementation. For flywheel-based inerters relying on rack-and-pinion and ball-screw mechanisms, it has been reported that dry friction effects dominate the response of the inerter for low frequency-low amplitude oscillations where the inerter responds as a metallic/friction damper (Papageorgiou and Smith 2005; Gonzalez-Buelga et al. 2016), while backlash effects are not as important. However, the various non-linear effects of the current/existing inerter devices, tailored for automotive applications, do not affect significantly the effectiveness of inerter-based vibration control in vehicle suspension systems [Wang and Su 2008; Li et al. 2012]. Similarly, in devising scaled-up inerter devices for the application at hand, it is important to ensure that a reasonably close to the ideal inerter behavior is observed for wind intensities above a certain threshold for which the full engagement/oscillation of the TMDI attached mass is required to ensure occupants' comfort as discussed in the following section.

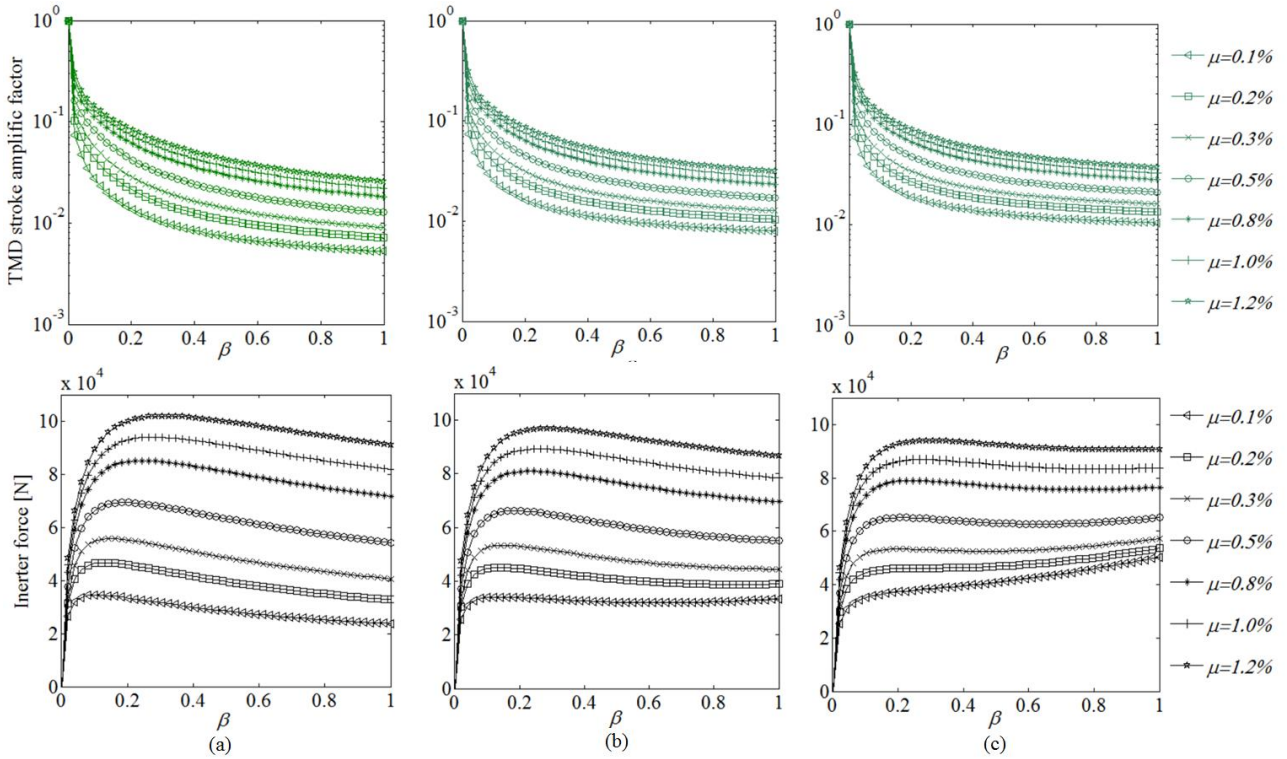

Fig. 5. Peak TMDI attached mass displacement over peak TMD attached mass displacement (upper panels), and peak inerter resisting force (lower panels) for different values of inertance ratio β and attached mass ratio μ for TMDI topologies (a)"-1", (b)"-2", and (c)"-3".

Table 1: Illustrative inerter flywheel sizing for three different TMDI cases examined in Fig.3.

	Inerter 1	*Inerter 2*	*Inerter 3*
TMDI topology	"-1"	"-2"	"-3"
*μ**	1%	1%	1%
*β**	69%	69%	69%
*Input energy***[kJ]	3.423	3.280	3.436
*Tangential flywheel velocity** [m/s]	50	50	50
*Flywheel thickness** [cm]	2.0	2.0	2.0
Flywheel mass [kg]	5.49	4.99	5.51
Flywheel radius[cm]	10.58	10.09	10.60

**quantities with pre-specified values; ** quantities obtained from structural analyses*

MEETING SERVICEABILITY CRITERIA IN NEW AND EXISTING TALL BUILDINGS

This section investigates the potential of the TMDI to meet user comfort criteria in new and in existing wind-excited tall buildings prescribed by typical building regulations. To this aim, reference is made to Fig. 6 which plots the peak top floor acceleration, $\max\{\ddot{x}_{74}\}$, of the primary structure in Fig.2 for

different values of the mean top floor wind velocity, V_{ref}, characterizing the intensity of the input wind action. Frequency-dependent design thresholds for occupants' comfort are superposed for residential and office buildings prescribed by current buildings codes and guidelines (Tamura et al. 2006; CNR 2008).

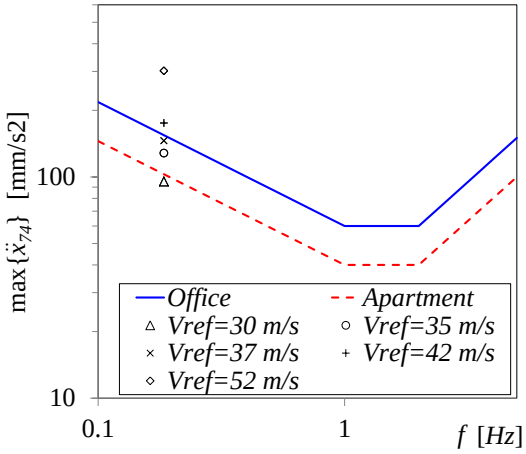

Fig. 6. Code-prescribed serviceability design thresholds and performance of the adopted primary structure for different V_{ref} values.

Focusing first on new tall buildings, suppose that it is sought to design a TMD(I)-based passive vibration control system to meet the serviceability design criteria in Fig.6 for the benchmark building in Fig.2 assuming V_{ref}=35m/s and apartment occupancy. It is seen in Fig.6 that the structure does not meet the users' comfort criterion of 102.90 mm/s^2 since $\max\{\ddot{x}_{74}\}$ =128.12 mm/s^2. Therefore, a RF of at least 128.12/102.90= 0.803 needs to be achieved by the vibration control system. Further, let the second raw of plots in Fig.3 be treated as design charts, interpreted in a performance-oriented rather than an assessment-oriented context (it is reminded that these charts do not meet any optimality criterion, however, the discussion here concerns relative performance and, on this basis, these charts are sufficient to draw valid conclusions). It is seen that the target RF=0.803 can be achieved by a classical TMD with an attached mass of 0.2% the total building mass. Nevertheless, the TMDI can achieve the same performance with half the attached mass, μ=0.1%, and with inertance ratio of β=0.24 for TMDI topology "-1", or β=0.10 for TMDI topology "-2", or β=0.06 for TMDI topology "-3". This arbitrarily taken design scenario illustrates numerically that the TMDI achieves the same structural performance with significantly smaller attached mass than the TMD leading to a more lightweight and cost-effective passive vibration control solution.

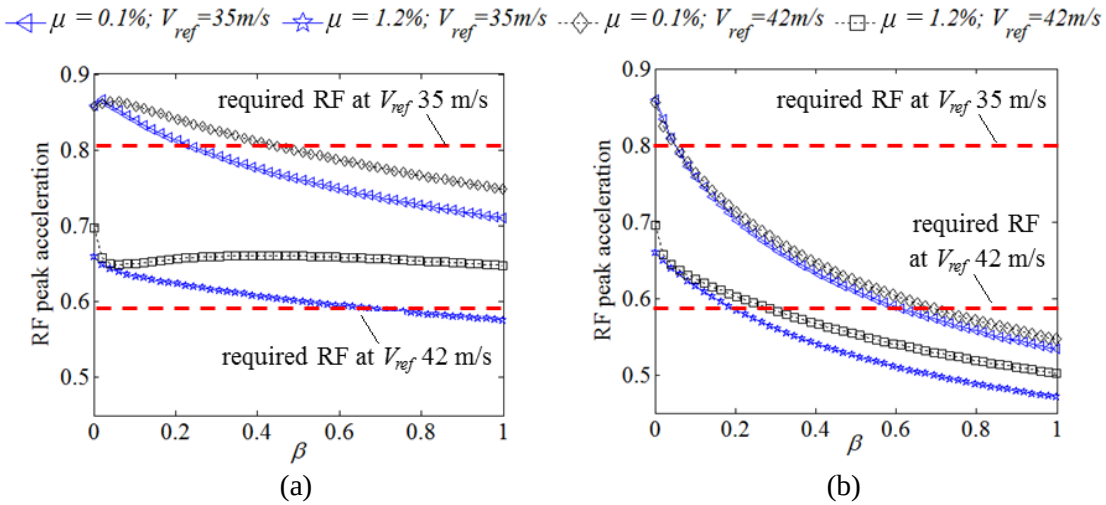

Fig. 7. Peak top floor acceleration of TMDI-equipped primary structure for different inertance ratio, β, and attached mass ratio, μ, values normalised by the corresponding peak values of the uncontrolled structure for two different design V_{ref} values and for TMDI topologies (a)"-1"and (b)"-3".

Turning the attention to the use of inerters to enhance the structural performance of existing TMD-equipped tall buildings, suppose that the site-specific design wind velocity, V_{ref}, increases from 35m/s to 42m/s during the lifetime of the same benchmark building. The latter scenario arises in case the exposure of the structure to wind effects increases (e.g., due to demolition of nearby tall building(s)), or in case the nominal design wind hazard increases due to climate change effects. The required RF in terms of peak top floor acceleration to meet the users' comfort criteria in Fig.6 reduces from 0.803 to 0.595 as indicated in Fig.7 by the horizontal red broken lines. In the last figure, the RFs for TMDI with "-1" and "-3" topologies are plotted versus the inertance ratio for a relatively small attached mass of μ=0.1% and for an excessively large attached mass of μ=1.2% for both the considered V_{ref} values. It is seen that the classical TMD with even the large μ=1.2% attached mass ratio cannot satisfy the users' comfort criteria for V_{ref}=42m/s. The same holds for the TMDI with topology "-1". However, for "-3" TMDI topology the users' comfort criteria for V_{ref}=42m/s can be met even with the small attached mass of μ=0.1% by incorporating an inerter with sufficiently large inertance (β>0.69%). Therefore, adding inerter devices in an appropriate topology can effectively enhance the performance of existing TMD-equipped tall buildings to meet serviceability criteria for higher wind velocities from the nominal value used in the original design without a change to the attached mass.

CONCLUDING REMARKS

The advantages and effectiveness of coupling inerter devices with linear passive TMDs to suppress excessive wind-induced oscillations in tall buildings in the across-wind direction have been numerically established and discussed. This was accomplished by furnishing pertinent numerical data involving a top-floor-TMD-equipped primary dynamical system accurately capturing the in-plane translational mode shapes and corresponding natural frequencies of a 74-storey square-plan benchmark building. A single linear inerter was incorporated to the considered system in various TMDI topologies introducing mass-amplification and higher-mode-damping effects. This was analytically achieved by adding appropriate inerter coefficient terms to certain diagonal and off-diagonal elements of the system mass matrix. The TMDI-equipped structure was exposed to wind forces modelled by a quasi-stationary spatially-correlated random field accounting for vortex shedding effects and structural analysis was undertaken in the frequency domain for several different attached mass values and for a wide range of inerter coefficients.

It was found that the TMDI reduces the peak top floor acceleration (i.e., the critical demand parameter in meeting serviceability criteria for occupants' comfort) beyond a same-weight TMD more effectively by considering: (I) smaller attached mass values, and (II) TMDI topologies in which the inerter spans more stories in linking the attached mass to the host structure. Condition (I) can be attributed to the mass amplification effect of the inerter which becomes more prominent for smaller TMD masses. Condition (II) is associated with the higher-mode-damping effect of the TMDI to the primary structure which was shown, by examining pertinent response acceleration transfer functions, to be more significant as more stories are spanned by the inerter (i.e., as the gyroscopic off-diagonal inerter terms in the mass matrix are further away from the main diagonal). It was further found that the above two conditions facilitate reductions to the peak top floor displacement as well supporting enhanced structural integrity. Moreover, it was demonstrated that the inclusion of the inerter achieves significant reductions to the TMD stroke which relaxes extensibility demands for the TMD damper and allows for reductions to the required clearance between the attached mass and host structure to avoid collisions.

More importantly from a practical viewpoint, it was numerically shown that: (i) the TMDI can meet code-prescribed serviceability design requirements by considering significantly smaller attached mass

(depending on the TMDI topology and inertance coefficient) compared to the TMD, enabling more lightweight construction and efficient material usage in the design of new tall buildings, and (ii) inerter devices can be used to upgrade existing TMD-equipped tall buildings, without changing the attached mass, to meet more stringent serviceability design requirements than those considered in the initial design due to site-specific climate change effects or changes to the surrounding built environment (i.e., increased wind exposure). To further support the feasibility of the above practical applications of the TMDI, numerical evidence were provided to argue that the developing inerter forces are of reasonable amplitude and can be locally accommodated by properly detailed inerter-structure connections. Moreover, it was illustrated through energy-based calculations that, even though inerter devices are not commercially available for control vibration applications in large-scale civil engineering structures, such inerters are physically and technologically feasible to manufacture by scaling-up current small-scale devices tailored for automotive applications.

Despite their usefulness to quantify the *relative* performance of the TMDI vis-à-vis the TMD for wind-induced vibration mitigation in tall buildings, it is emphasized that the herein reported numerical data are based on sub-optimal TMDI properties. Optimum TMDI design to meet code-prescribed users' comfort criteria in wind-excited tall buildings accounting for potential effects of torsional vibration modes (Tse *et al.* 2007) will be addressed by the authors in a subsequent publication. Furthermore, throughout this study, the availability of ideal linear inerters has been assumed which is a common assumption in the relevant literature (e.g. Takewaki et al. 2013; Lazar et al. 2014; Marian and Giaralis 2014), although it is known that current (small-scale) inerter devices may depart from this behavior outside a particular device-dependent and application-dependent frequency range (e.g. Papageorgiou and Smith 2005; Swift et al. 2013; Gonzalez-Buelga et al. 2016). In this regard, accounting for the influence of non-linear inerter behavior to the effectiveness of TMDIs for tall building wind vibration mitigation warrants further research which need to be supported by prototyping and characterization of large-scale inerters. To this end, it is envisioned that this study will not only further familiarize the civil/structural engineering community to the potential benefits of considering inerter devices for vibration control in TMD-equipped structures, but also justify the pursue of experimental research to develop inerters suitable for large-scale civil engineering structures.

ACKNOWLEDGEMENTS

This work has been funded by EPSRC in UK, under grant EP/M017621/1. The authors gratefully acknowledge this financial support. The authors are further grateful to Prof. Malcolm Smith (University of Cambridge), Prof. Keith Pullen (City, University of London), and Prof. Simon Neild (University of Bristol) for the discussions on the feasibility of large-scale inerter devices for civil engineering structures that informed relevant parts of the paper.

REFERENCES

Bernardini, E., Spence, S.M.J., Kwon, D.K. and Kareem, A. (2015). "Performance-Based Design of High-Rise Buildings for Occupant Comfort." *J. Struct. Eng.*, 141(10), 10.1061/(ASCE)ST.1943-541X.0001223, 04014244.

Chopra, A.K. (2000). *Dynamics of Structures: Theory and Applications to Earthquake Engineering*, 2nd Edition, Prentice-Hall, U.S.

Ciampoli, M. and Petrini, F. (2012). "Performance-Based Aeolian Risk assessment and reduction for tall buildings." *Prob. Eng. Mech.*, 28,75–84.

CNR - Consiglio Nazionale delle Ricerche (2008). CNR-DT 207/2008: Istruzioni per la valutazione delle azioni e degli effetti del vento sulle costruzioni. (in Italian).

Davenport, A.G. (1964). "Note on the distribution of the largest value of a random function with application to gust loading." *Proc. of the Institution of Civil Engineers*, 28(2), 187-196.

De Angelis, M., Perno, S. and Reggio, A. (2012). "Dynamic response and optimal design of structures with large mass ratio TMD." *Earthquake Eng. Struct. Dyn.*, 41, 41–60.

Giaralis, A. and Taflanidis A.A. (2015). "Reliability-based design of tuned-mass-damper-inerter (TMDI) equipped stochastically support excited structures*." Proc., 12th Int. Conf. on Applications of Statistics and Probability in Civil Engineering*, T. Haukass, ed., paper #538, The University of British Columbia, ISBN 978-0-88865-245-4.

Gonzalez-Buelga, A., Clare, L.R., Neild, S.A, Jiang, J.Z. and Inman, D.J. (2015). "An electromagnetic inerter-based vibration suppression device." *Smart. Mater. Struct.*, **24**, 10.1088/0964-1726/24/5/055015.

Gonzalez-Buelga, A., Lazar, I., Jiang, J.Z., Neild, S.A. and Inman, D.J. (2016). "Assessing the effect of nonlinearities on the performance of a Tuned Inerter Damper." *Struct.* Control Health Monit., DOI: 10.1002/stc.1879.

Karavasilis, T.L., Kerawala, S., Hale, E. (2011). "Hysteretic model for steel energy dissipation devices and evaluation of a minimal-damage seismic design approach for steel buildings." *J. Constr. Steel Res.*, 70, 358-367.

Kareem, A. (1982). "Across wind response of buildings", *J. Struct. Div.*, ASCE 108 (ST4), 869–887.

Kareem, A., Kijewski, T. and Tamura, Y. (1999). "Mitigation of motions of tall buildings with specific examples of recent applications." *Wind Structures*, 2(3), 201-251.

Krenk, S. and Høgsberg, J. (2016). "Tuned resonant mass or inerter-based absorbers: unified calibration with quasi-dynamic flexibility and inertia correction." *Proc. of the Royal Society A Mathematical Physical and Engineering Sciences*, 472(2185), 20150718.

Kwok, K.C.S, Hitchcock, P.A. and Burton, M.D. (2009). "Perception of vibration and occupant comfort in wind-excited tall buildings." *J. Wind Eng. Ind. Aerodyn.*, 97, 368–380.

Lazar, I.F., Neild, S.A. and Wagg D.J. (2014). "Using an inerter-based device for structural vibration suppression." *Earthquake Eng. Struct. Dyn.*, 43(8), 1129-1147.

Li., C., Liang, M., Wang, Y., Dong, Y. (2012). "Vibration suppression using two terminal flywheel. Part I: Modeling and Characterization." *J. Vibr. Contr.*, 18(8),1096-1105.

Li, Q., Cao, H., Li, G., Li, S. and Liu, D. (1999). "Optimal design of wind-induced vibration control of tall buildings and high-rise structures." *Wind Struct.*, 2(1), 69-83.

Liang, S., Liu, S., Li, Q.S., Zhang, L. and Gu, M. (2002). "Mathematical model of across-wind dynamic loads on rectangular tall buildings." *J. Wind Eng. Ind. Aerodyn.*, 90, 201-251.

Marian, L. and Giaralis, A. (2013). "Optimal design of inerter devices combined with TMDs for vibration control of buildings exposed to stochastic seismic excitations." *Proc,.11th ICOSSAR Int. Conf. on Structural Safety and Reliability*, G. Deodatis, B.R. Ellingwood, D.M. Frangopol, ed., CRC Press, NY, 1025-1032.

Marian, L. and Giaralis, A. (2014). "Optimal design of a novel tuned mass-damper–inerter (TMDI) passive vibration control configuration for stochastically support-excited structural systems." *Prob. Eng. Mech.*, 38, 156–164.

Papageorgiou, C. and Smith, M.C. (2005). "Laboratory experimental testing of inerters." *Proc., 44th IEEE Conf. Decision Control*, 3351-3356.

Petrini, F. and Ciampoli, M. (2012). "Performance-based wind design of tall buildings." *Structure & Infrastructure Engineering - Maintenance, Management, Life-Cycle Design & Performance*, 8(10), 954-966.

Pullen, K.R. and Dhand, A. (2014). "Mechanical and electrical flywheel hybrid technology to store energy in vehicles." In: *Alternative Fuels and Advanced Vehicle Technologies for Improved Environmental Performance*, R. Folkson, ed., Woodhead Publishing ltd, Cambridge, U.K.

Rana, R. and Soong, T.T. (1998). "Parametric study and simplified design of tuned mass dampers." *Eng. Struct.*, 20(3), 193-204.

Satake, N., Suda, K., Arakawa, T., Sasaki, A. and Tamura, Y. (2003). "Damping evaluation using full-scale data of buildings in Japan." *J. Struct. Eng.*, 10.1061/(ASCE)0733-9445(2003)129:4(470).

Simiu, E., and Scanlan, R.H. (1978). "*Wind effects on structures*". John Wiley & Sons Inc., New York.

Smith, M.C. (2002). "Synthesis of Mechanical Networks: The Inerter." *IEEE Trans. Automat. Control*, 47(10), 1648-1662.

Soong, T.T. and Grigoriu, M. (1993). *Random vibration of mechanical and structural systems*, Prentice-Hall, New Jersey.

Spence, S.M.J. and Gioffrè, M. (2012). "Large scale reliability-based design optimization of wind excited tall buildings." *Prob. Eng. Mech.*, 28, 206-215.

Spence, S.M.J. and Kareem, A. (2014). "Tall buildings and damping: A concept-based data-driven model." *J. Struct. Eng.*, DOI: 10.1061/(ASCE)ST.1943-541X.0000890.

Swift, S.J., Smith, M.C., Glover, A.R., Papageorgiou, C., Gartner, B. and Houghton, N.E. (2013). "Design and modelling of a fluid inerter." *Intern. J. Control*, 86(11), 2035–2051.

Takewaki, I., S. Murakami, S. Yoshitomi, and M. Tsuji (2012). "Fundamental mechanism of earthquake response reduction in building structures with inertial dampers." *Struct. Control Health Monitor.*, 19(6), 590-608.

Tamura, Y., Kawana, S., Nakamura, O., Kanda, J. and Nakata S. (2006). "Evaluation perception of wind-induced vibration in buildings." *Proceedings of the Institution of Civil Engineers - Structures and Buildings*, 159(5), 283-293.

Tse, K.T., Kwok, K.C.S., Hitchcock, P.A., Samali, B., and Huang, M.F. (2007), "Vibration Control of a Wind-Excited Benchmark Tall Building with Complex Lateral-Torsional Modes of Vibration", *J. Adv. Struct. Eng.*, 10, 283-304.

Tse, K., Kwok, K., and Tamura, Y. (2012). "Performance and Cost Evaluation of a Smart Tuned Mass Damper for Suppressing Wind-Induced Lateral-Torsional Motion of Tall Structures." *J. Struct. Eng.*, 10.1061/(ASCE)ST.1943-541X.0000486, 514-525.

Vickery, B.J. and Basu, R.I. (1983). "Across-wind vibrations of structures of circular cross-section. Part 1. Development of a mathematical model for two-dimensional conditions", *J. Wind Eng. Ind. Aerodyn.*, 12, 49-73.

Wang, F.C., and Su, W.J. (2008). "Impact of inerter nonlinearities on vehicle suspension control," *Vehicle System Dyn.*, 46, 575-595.

Wang, F.C., Hong, M.F. and Lin, T.C. (2011). "Designing and testing a hydraulic inerter." *Proc. Inst. Mech. Eng. Part C J. Mech. Eng. Sci.*, 1(265), 66–72.

Wang, J.F., Lin C.C. and Lian C.H. (2009). "Two-stage optimum design of tuned mass dampers with consideration of stroke." *Struct. Control Health Monitor.*,16,55-72.

Warburton, G.B. (1982). "Optimal absorber parameters for various combinations of response and excitation parameter." *Earthquake Eng. Struct. Dyn.*, 10, 381-400.

Wu, J.C., Yang, J.N. and Schmitendorf, W.E. (1998). "Reduced-order H∞ and LQR control for wind-excited tall buildings." *Eng. Struct.*, 20(3), 222-236.

Yang, J., Agrawal, A., Samali, B., and Wu, J. (2004). "Benchmark Problem for Response Control of Wind-Excited Tall Buildings." *J. Eng. Mech.*, 130(4), 437-446.